Magnetic Phase Diagram of $Cr_{1-x}Ir_x$ alloys

PR Fernando, CJ Sheppard, ARE Prinsloo[1] and AM Strydom

Department of Physics, University of Johannesburg, PO Box 524, Auckland Park, 2006

Author e-mail address: alettap@uj.ac.za

Abstract. Cr alloyed with group-8 nonmagnetic transition metals Ir, Os, Ru, Re and Pt show large anomalies of magnetic origin at the phase transition temperatures. Doping with these metals increase the electron to atom ratio of Cr and their magnetic phase diagrams contain the commensurate (C) spin density wave (SDW) phase, as well as the paramagnetic (P) phase, the transverse (T) incommensurate (I) SDW and longitudinal (L) ISDW phases. A triple point exists where the ISDW, CSDW and P phases coexist, while the CSDW phase is observed for impurity concentrations (x) above the triple point concentration (x_L). The magnetic phase diagrams of both CrRe and CrRu show interesting features for $x >> x_L$, including possible superconducting properties and quantum critical behaviour. In this contribution we extend these investigations to the phase diagram of $Cr_{1-x}Ir_x$, previously not determined for $y > 0.04$. A polycrystalline $Cr_{1-x}Ir_x$ sample series, with $0.02 < x < 0.14$, was prepared and characterized using scanning electron microscopy, electron microprobe analysis and X-ray diffraction. These reveal that the alloys with $x \leq 0.12$ are homogenous in composition and single-phase. Electrical resistivity (ρ) measurements as function of temperature (T) for $2K < T < 1000K$ was used to obtain the magnetic transition temperatures of the samples and determine the magnetic phase diagram of the $Cr_{1-x}Ir_x$ alloy system for $x > 0.04$.

1. Introduction

In Cr and its alloys the electron and hole Fermi surfaces nest on cooling through the Néel temperature (T_N) resulting in the formation of the spin-density-wave (SDW) when the antiferromagnetic (AFM) phase is entered. This nesting decreases the energy of the system through electron-hole pair condensation and results in the appearance of SDW energy gaps at the Fermi surface in certain directions of k-space on cooling through T_N. The first parameter of importance in influencing the formation of the SDW is the effect of electron concentration on the area of the electron and hole Fermi surface sheets that nests [1]. The nesting area, and concomitantly the stability of the SDW state, depends on the electron concentration per atom (e/a) which can easily be tuned by alloying Cr ($e/a = 6$) with elements having different e/a ratios. Diluents that increase the electron concentration in Cr alloys, such as Mn ($e/a = 7$) as well as group-8 nonmagnetic transition metals, increase the area of the electron sheet, resulting in a better nesting of the Fermi surface sheets and the formation of a commensurate (C) SDW phase at certain diluent concentrations.

Of special interest is Cr alloys with group-8 nonmagnetic transition metals Ru, Os, Rh, Ir and Pt. These alloys show large anomalies of magnetic origin at the phase transition temperatures [1]. These impurities increase the electron to atom (e/a) ratio of Cr and therefore the phase diagrams of the Cr alloys with group-8 nonmagnetic transition metals contain the commensurate (C) SDW phase, as well as the paramagnetic (P) phase, the transverse (T) incommensurate (I) SDW and longitudinal (L) ISDW

phases. A triple point exists on the magnetic phase diagrams of these alloys were the ISDW, CSDW and P phases coexist [1]. For impurity concentrations (x) below the triple point concentration (x_L) the dilute Cr alloys with group-8 impurities LISDW, TISDW and P phases are observed, while for $x > x_L$ we also observe a CSDW phase. The spin-flip phase transition (at temperature T_{SF} defined as the transition temperature between LISDW and TISDW magnetic phases), the Néel transition at temperature (T_N) of Cr and the ISDW-CSDW magnetic phase transition at temperature T_{IC} of certain Cr alloys with group-8 nonmagnetic transition metals are first order transitions and hysteresis effects can be observed in certain of the physical properties [1,2].

Much of the previous work on the $Cr_{100-x}Ir_x$ system focussed on alloys close to x_L [1,9] and little attention was given to high diluent concentrations. Since the magnetic phase diagrams of many Cr alloys with group-8 metals show very interesting properties [1], it is surprizing that the Cr-Ir magnetic phase diagram has not been fully explored and is still unknown for concentrations above 4 at.% Ir [10]. Fascinating features of the magnetic phase diagrams of both the Cr-Re and Cr-Ru systems include possible superconducting properties, as well as quantum critical behaviour [1,3,4] for $x >> x_L$. These properties are strongly aligned with current interests as is reflected in recent literature [5,6,7,8]. Extending these investigations to the Cr-Ir system will prove most interesting and in this paper the first step in doing this is taken by determining the magnetic phase diagram of the Cr-Ir system at higher diluent come, which will give much scope for future research.

2. Experimental

The polycrystalline binary $Cr_{1-x}Ir_x$ alloys, with $0.02 \leq x \leq 0.14$ were prepared by arc melting in a purified argon atmosphere from Cr and Ir of mass fractional purities 99.999% and 99.99%, respectively. The constituent metals were melted fifteenth times in total, turning it upside down between melts with two crushes after every five melts in order to improve the homogeneity. Samples were prepared as cast and for comparison certain samples were annealed at 1000°C for 7 days. The complex nature of the chemical phase diagram of Cr-Ir indicate possible difficulties in preparing single phase Cr-Ir alloys, as was outlined by Waterstrat *et al.* [11]. For this reason it was essential to characterize the samples structurally. Powder X-ray diffraction (XRD) analyses, using Cu-K_α were used to confirm whether the samples were single or multi-phase. The approximate chemical compositions of the individual alloys were obtained using a scanning electron microprobe (SEM) and energy-dispersive X-ray spectrometry (EDS). The actual elemental composition and homogeneity were determined using electron microprobe analyses. Electrical resistivity (ρ) were measured in the range $2 \leq T \leq 380$ K, using standard Physical Properties Measurement System (PPMS) incorporating appropriate measuring options. Resistivity measurements for the temperature range 273 K − 1000 K were performed in an inert environment using the standard dc-four probe method with Keithley instrumentation. In order to eliminate the thermal EMF the sample current was reversed for each set of readings [12].

3. Results and discussion

Figure 1 (a) and (b) shows the XRD patterns for the as-cast $Cr_{0.90}Ir_{0.10}$ and $Cr_{0.86}Ir_{0.14}$ samples, respectively, together with the XRD pattern for pure Cr. The XRD pattern for $Cr_{0.90}Ir_{0.10}$ was compared to the Joint Council of Powder Diffraction Database for pure Cr and only the primary reflections [110], [200], [211] and [220] were obtained. These reflections were shifted to lower angles with substitution of Ir in the lattice, corresponding to an increase in the lattice parameter. This is expected as the Ir atoms are larger than Cr atoms. The lattice parameter increased from 0.28839 nm (pure Cr) to 0.3092 nm for the $Cr_{0.90}Ir_{0.10}$ alloy. On analyzing the XRD pattern for the $Cr_{0.86}Ir_{0.14}$ alloy in a similar manner, additional reflections were identified that can be associated with that of Cr_3Ir (A15-phase), which was previously described by Waterstrat *et al.* [11]. Figure 2 gives the lattice parameters for $Cr_{1-x}Ir_x$ alloys with $0 \leq x \leq 0.12$. Linear behaviour is observed in this concentration range.

The backscattered-electron micrographs of the as-cast $Cr_{0.90}Ir_{0.10}$ and $Cr_{0.86}Ir_{0.14}$ alloys are shown in figure 3 (a) and (b), respectively. The images for these samples are very similar indicating uniform surface morphology with no distinguishable features that can be associated with other Cr-Ir phases.
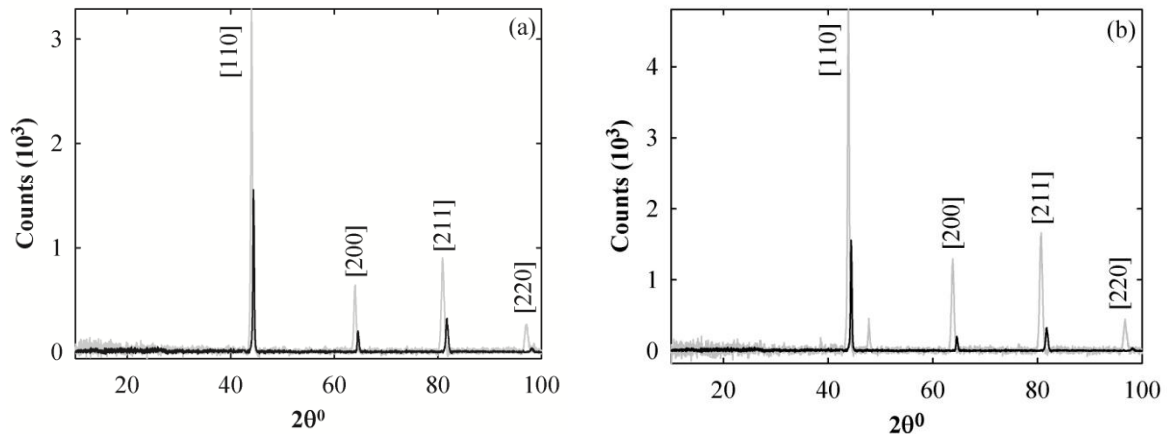

Figure 1. The XRD pattern for the (a) $Cr_{0.90}Ir_{0.10}$ and (b) $Cr_{0.86}Ir_{0.14}$ alloys are shown in grey, together with the pattern expected for pure Cr shown in black. The (*hkl*) Miller indices of the various reflections obtained from the JCPDD expected for the profile of bcc Cr are indicated.
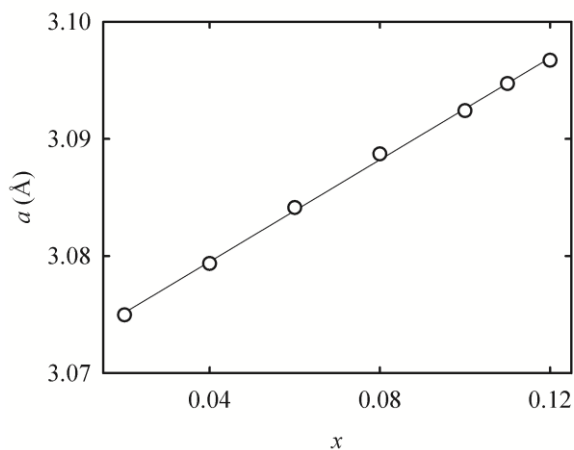

Figure 2. The lattice constants (*a*) as function of *x* for various $Cr_{1-x}Ir_x$ alloys.

Microprobe analysis for the $Cr_{0.90}Ir_{0.10}$ sample indicate homogeneous composition with a Cr concentration of (90.0 ± 0.6) at.% and Ir of (10.1 ± 0.6) at.%. For the $Cr_{0.86}Ir_{0.14}$ sample microprobe analysis also indicates homogeneous composition with a Cr concentration of (85.4 ± 0.7) at.% and Ir of (14.6 ± 0.7) at.%. The light and the dark regions observed in the images shown in figure 3 (a) and (b) differ only slightly in concentration. In an attempt to improve the quality of the samples it was annealed, but this resulted in the deterioration of sample quality. Figure 4 (a) and (b) shows the XRD and backscattered-electron image of the $Cr_{0.90}Ir_{0.10}$ sample after annealing. The XRD pattern of the annealed $Cr_{0.90}Ir_{0.10}$ sample show several additional peaks, not associated with the bcc phase expected in Cr alloys.

Comparing the backscattered-images of figures 3 (a) and 4 (b) for the $Cr_{0.90}Ir_{0.10}$ sample, a significance difference is observed between the as-cast and annealed samples. The annealed sample is of inhomogeneous morphology showing needle-like structures on a smooth background, comparable to results found by Waterstat *et al.* [11]. According to EDS analysis, in this case the needle like structures in the annealed $Cr_{0.90}Ir_{0.10}$ sample has Cr and Ir concentrations of (81.2 ± 0.1) at.% and (18.8 ± 0.2) at.%, respectively. However, the background has Cr and Ir concentrations of (94.4 ± 0.7) at.% and (5.6 ± 0.7) at.%, respectively. After annealing the backscattered-image of the $Cr_{0.86}Ir_{0.14}$ sample shows no needle-like structures, only large sections of a light regions with (81.5 ± 0.6) at.%

Cr and (18.5 ± 0.6) at.% Ir, together with smaller dark regions with (93.0 ± 0.5) at.% Cr and (7 ± 1) at.% Ir. Interestingly in these two samples the background/dark regions, as well as the needle-like/light regions have similar concentrations, independent of the initial diluent concentrations.

The $\rho(T)$ curves for $Cr_{1-x}Ir_x$ alloys, with $0.02 \leq x \leq 0.14$ are shown in figure 5 (a) and (b). Well defined anomalies in the form of clear minima followed by prominent domes are seen in all the $\rho(T)$ curves for alloys with $x < 0.14$. This behaviour is associated with the formation of the SDW on entering the antiferromagnetic phase on cooling through the Néel temperature [1]. The sudden increase in resistivity on cooling through T_N finds its origin in the condensation of electron and hole Fermi surfaces during the nesting process on SDW formation. This leads to a reduction in the charge carriers available for conduction resulting in an increase in resistivity just below T_N [1]. T_N is often defined for Cr and its dilute alloys as the temperature of the minimum in $d\rho/dT$ accompanying the magnetic phase transition [1]. This definition was implemented for the present study of the $Cr_{1-x}Ir_x$ system. The single-phase bcc alloys reveal one clear transition at T_N. However, the multi-phase alloy with $x = 0.14$ shows two anomalies in $\rho(T)$, as can be seen in figure 5 (b). These are associated with the two different phases that would be in agreement with the observations in the XRD and backscattered images of this sample. The experimental error in the absolute value of ρ amounts to 5% and originates mainly from errors in determining the sample dimensions, while the instrumentation used permitted a resistivity resolution of 0.5%.
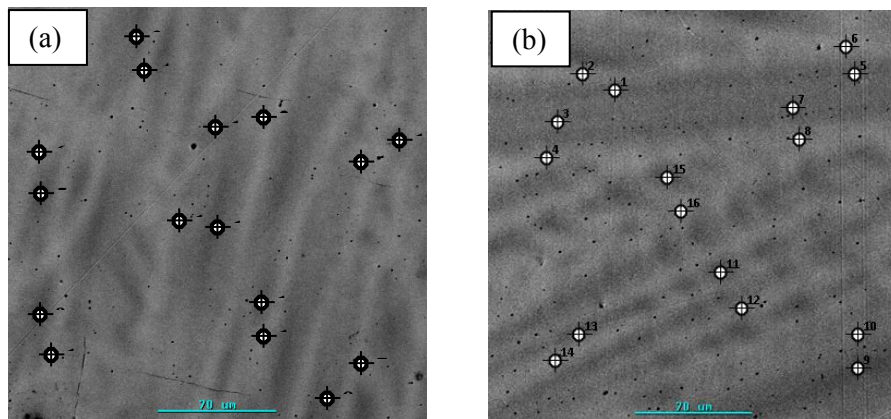

Figure 3. The backscattered-electron images for the as cast (a) $Cr_{0.90}Ir_{0.10}$ and (b) $Cr_{0.86}Ir_{0.14}$ alloys. Positions where the concentrations in light and dark phases were determined using EDS are indicated.

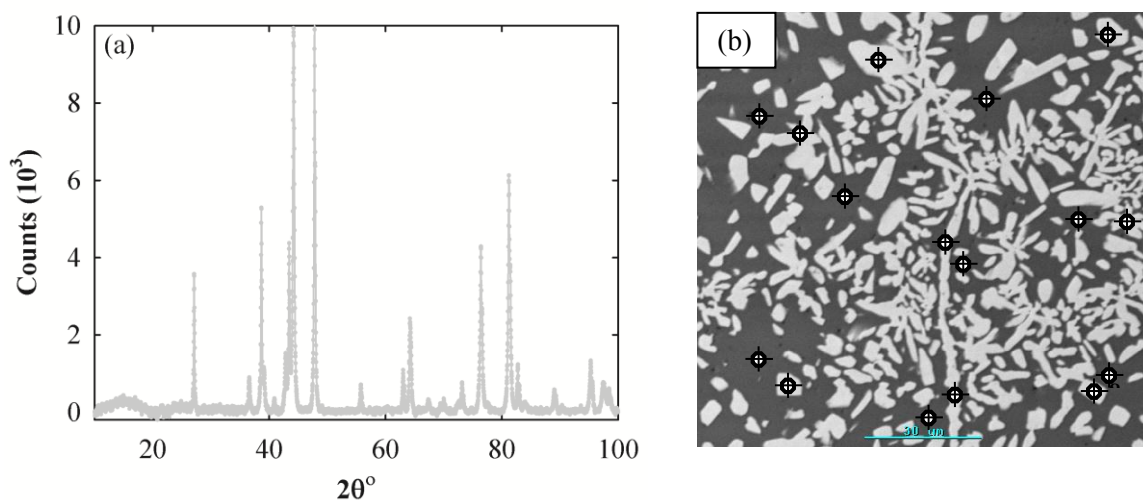**Figure 4.** The (a) XRD pattern and (b) backscattered-electron image for the annealed $Cr_{0.90}Ir_{0.10}$ alloy.

The positions where the concentrations in the light and dark phases were determined using EDS are indicated in (b).

Figure 6 shows the magnetic phase diagram constructed from the T_N-values obtained from the current $\rho(T)$ measurements together with those obtained in previous studies [9,10,13-16], as a function of Ir concentration. The error in the current T_N values falls within the size of the data points. The solid lines are guides to the eye through the data points. It is evident that the current results correspond well with those previously obtained on this alloy system. The present study extends results to much higher Ir diluent concentrations than previously determined [9]. The magnetic phase diagram obtained for Cr-Ir alloy system resembles the typical behaviour of Cr alloys with group-8 metals, similar to that observed for Cr-Ru and Cr-Re.
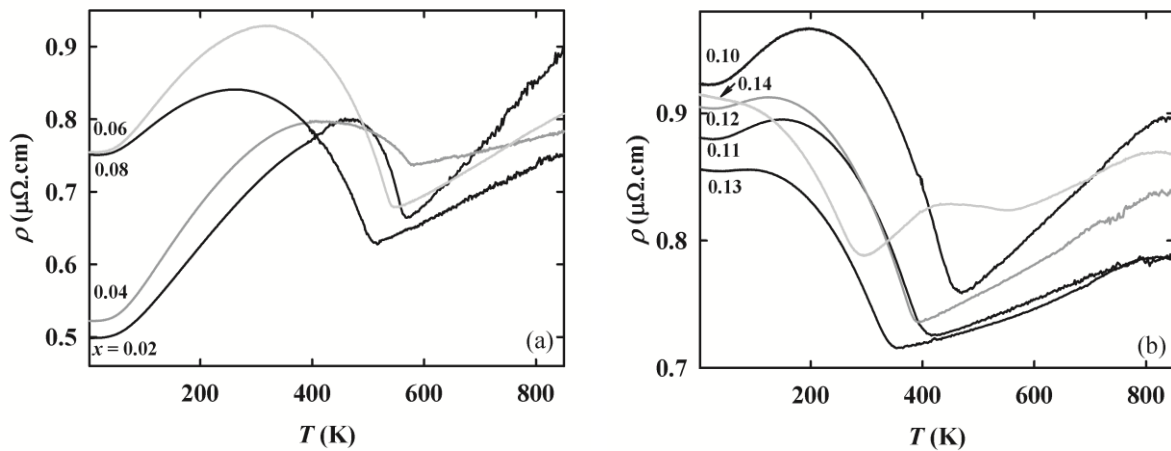

Figure 5 (a) and (b). The temperature dependence of the electrical resistivity, ρ, of $Cr_{1-x}Ir_x$ alloy system. The values of x associated with the various curves are indicated on the graphs.
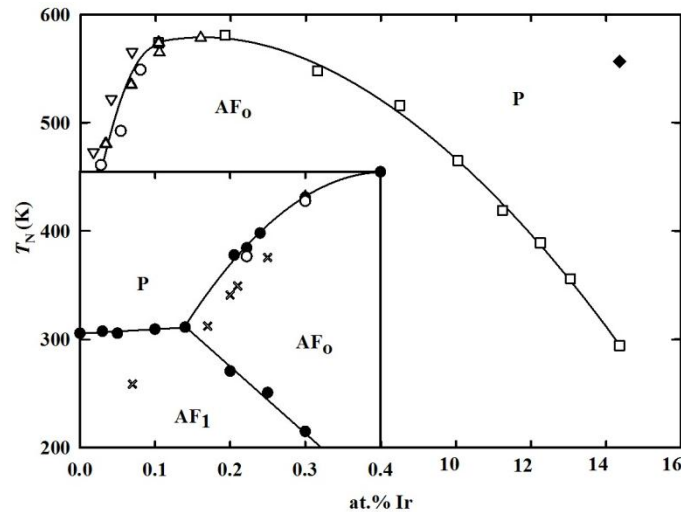

Figure 6. The magnetic phase diagram for the $Cr_{1-x}Ir_x$ alloy system as function of the Ir concentration, showing T_N values obtained through electrical resistivity in present study (□). The second transition temperature observed for the $Cr_{0.86}Ir_{0.14}$ sample are indicated by ◆. Data points from previous studies indicated on the figure: Fukamichi *et al.* [9] (△), Yakhmi *et al.* [14] (O), De Young *et al.* [15] (▽), Butylenko *et al.* [17] (●) and Martynova *et al.* [10] (✖). The error in the T_N values obtained from the current study falls within the size of the data points. The solid lines are guides to the eye.

4. Conclusion.

The magnetic phase diagram for the $Cr_{1-x}Ir_x$ alloys system was for the first time determined to concentrations as high as 12 at.% Ir. The present results compare well with that previously obtained [10,13-17] on this alloy system for $x < 0.04$ and the general behaviour is similar to that observed for other Cr alloys with group-8 non-transition metals such as Cr-Ru and Cr-Re [1]. These results will be extended to include the T_N-values obtained from additional physical properties measurements, firstly for $T < 400$ K and then in the second stage for $T > 400$ K.

This project has addressed the fundamental questions regarding the behaviour of the Cr-Ir magnetic phase diagram at high diluent concentrations necessary to evolve the research on this alloy system to a higher level. This will include investigations into quantum critical behaviour and possible superconductivity in the Cr-Ir alloy system, in line with current interests as is reflected in recent literature [5,6,7,8].

References

[1] Fawcett E, Alberts HL, Galkin VY, Noakes DR and Yakhmi JV 1994 *Rev. Mod. Phys.* **66** 25
[2] Fawcett E 1988 *Rev. Mod. Phys.* **60** 209
[3] Jacobs BS, Prinsloo ARE, Sheppard CJ and Strydom AM 2011 *Proceedings of SAIP* 105
[4] Reddy L, Alberts HL, Strydom AM, Prinsloo ARE and Venter AM 2008 *J. Appl. Phys.* **103** 07C903-1
[5] Yeh A, Soh Y-A, J Brooke J, Aeppli G, Rosenbaum TF and Hayden SM 2002 *Nature* **419** 459
[6] Lee M, Husmann A, Rosenbaum TF and Aeppli G 2004 *Phys. Rev. Lett.* **92** 187201
[7] Jaramillo R, Feng Y, Wang J and Rosenbaum TF 2010 *Proc. Nat. Acad. of Sci. USA (PNAS)* **107** 13631
[8] Sheppard CJ, Prinsloo ARE, Alberts HL and Strydom AM 2011 *J. Appl. Phys.* **109**(7) 07E104
[9] Martynova J, Alberts HL and Smit P 1998 *J. Magn. Magn. Mat.* **197** 345
[10] K Fukamichi and Siato H 1975 *J. Less Common Met.* **40** 357
[11] Waterstat RM and Manuszewski RC 1973 *J. Less Common Met.* **32** 79
[12] Gopalakrishnan IK,Yakhmi JV and Iyer RM 1984 *J. Magn. Magn. Mat.* **46** 207
[13] Arajs S, Rao KV, Åström HU and De-Young F.Tice 1973 *Physica Scripta*.vol.8 109-112
[14] Yakhmi JV, Gopalakrishnan IK and Iyer RM 1983 *J. Less Common Met.* **91** 327-331
[15] De Young F.Tice, Arajs S and Anderson EE 1971 *Amer. Inst. Phys. Conf. Proc. Magn and Magn. Mat*. **5** 517.
[16] Butylenko AK and Nevadcha VV 1980 *Dokl. Akad. Nauk Ukr.SSR* **5**A 67